



# Skin viscoelasticity studied *in vitro* by microprobe-based techniques



T. Jee, K. Komvopoulos\*

Department of Mechanical Engineering, University of California, Berkeley, CA 94720, USA

## ARTICLE INFO

### Article history:

Accepted 8 October 2013

### Keywords:

Deformation  
Indentation  
Skin  
Stiffness  
Viscoelasticity

## ABSTRACT

Time-dependent deformation of porcine skin was studied *in vitro* using specialized microprobe instruments. The deformation behavior of stratum corneum, dermis, and whole skin is examined in the context of results of creep strain, elastic stiffness, and viscoelastic constants obtained in terms of the hold time, loading/unloading rate, and maximum indentation depth (load). Skin time-dependent deformation is significantly influenced by dermis viscoelasticity up to a critical indentation depth (load) beyond which it is controlled by the outermost hard epidermis, particularly stratum corneum. Skin viscoelastic behavior under constant load (creep) and constant displacement (stress relaxation) is interpreted in the light of phenomenological observations and experimental trends.

© 2013 Published by Elsevier Ltd.

## 1. Introduction

Skin viscoelasticity is critical to its protective function, plays a key role in cosmetic product development, and has significant societal implications (aging effect). The viscoelastic behavior of skin is influenced by various factors, including sex, ethnicity, age, and nutrition (Archer, 2010; McGrath and Uitto, 2010), disease stage, and stress state (Frick et al., 2001; Butz et al., 2012). Although medical and clinical studies of the mechanical properties of healthy and injured skin began several decades ago (Glaser et al., 1965; Fry et al., 1964; Gibson et al., 1969), *in vitro* test methods relying on microprobe-based mechanical techniques, such as micro/nanoindentation, which are capable of measuring the mechanical properties of individual skin layers at cellular and sub-cellular levels can be found only in a few recent experimental (Yuan and Verma, 2006; Geerligs et al., 2011; Crichton et al., 2011, 2013) and numerical (Groves et al., 2012) investigations. Thus, knowledge of the effects of individual skin layers to the overall mechanical behavior of skin at the microscale, particularly viscoelasticity, is rather sparse and empirical.

Emerging microneedle-based approaches, such as transdermal drug and vaccine delivery or blood and interstitial fluid sampling, require understanding of skin viscoelasticity at cellular (on the order of 10  $\mu\text{m}$ ) and sub-cellular levels. However, most previous studies of the mechanical behavior of skin have focused on either a single skin layer or whole skin (Shergold et al., 2006; Holt et al., 2008), relying on continuum treatments (Groves et al., 2012) or macroscale experimental techniques (Frick et al., 2001; Shergold et al., 2006; Holt et al., 2008; Lamers et al., 2013), which do not account for anatomical differences and the scale dependence of skin viscoelasticity. For example, vaccine delivery to the

targeted immune cells at the intended injection site greatly depends on the depth of microneedle penetration, which is a strong function of the viscoelastic behavior of each skin layer.

The main objective of this study is to obtain insight into the viscoelastic behavior of skin at the microscale using micro/nanoindentation techniques and to identify the effect of layer constituents on the overall viscoelastic response of skin. Time-dependent deformation results yielding information about the elastic stiffness and viscoelastic parameters of the epidermis, dermis, and whole skin are presented for a range of loading/unloading rate, hold time, depth rate (indentation speed), and maximum depth (load). These measurements combined with histology results provide insight into the time-dependent deformation intricacies of the skin.

## 2. Experimental methods

### 2.1. Sample preparation

Because of histological, physiological, and immunological similarities of porcine skin and human skin (Schmook et al., 2001; Avon and Wood, 2005; Zak et al., 2011), skin samples of euthanized 8–12 months old American Yorkshire pigs were tested within 5 h from acquisition. The samples were embedded in a filtered paper soaked in 0.9% NaCl solution and the hair was removed with a surgical knife. Samples containing the stratum corneum and a significant portion of the epidermis were obtained by shearing off an outer skin layer of a few micrometers thickness with a surgical blade. This method is preferred over chemical isolation techniques because it allows for tissue separation with minimal damage and without undesirable chemical effects. Dermis samples were obtained from whole skin samples by shearing off most of the hypodermis with a surgical knife. After testing, the samples were frozen on dry ice.

### 2.2. Histology analysis

For cross-sectional histology studies, whole skin samples were embedded in an optimal-cutting-temperature compound (TissueTek, Elkhart, IN) on dry ice and

\* Corresponding author. Tel.: +1 510 642 2563; fax: +1 510 642 5539.  
E-mail address: [kyriakos@me.berkeley.edu](mailto:kyriakos@me.berkeley.edu) (K. Komvopoulos).

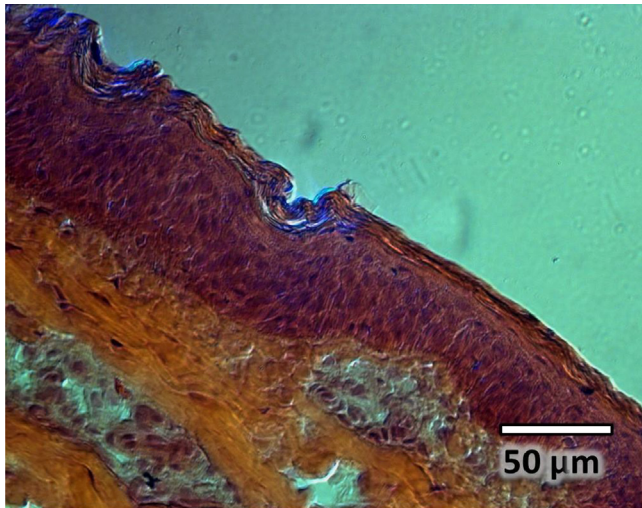


**Fig. 1.** Cross-sectional image of skin obtained after scratching under a load of 50 mN.

kept at a temperature of  $-62\text{ }^{\circ}\text{C}$  until testing. Then,  $10\text{-}\mu\text{m}$ -thick specimens were sectioned from the skin samples and stained with hematoxylin and eosin following a standard protocol. Cross-sectional imaging (Fig. 1) confirmed that other than localized damage induced by the mechanical probe during testing, removing an outer layer of a few micrometers thickness with a surgical blade and subsequently freezing the obtained sample were not destructive to the tissue histology.

### 2.3. Microprobe-based mechanical testing

Low-load/small-depth indentation tests were performed with a surface force microscope (SFM) described elsewhere (Supporting information). All SFM tests were performed with a conospherical diamond tip of  $1\text{ }\mu\text{m}$  radius. Approximately 10 samples were used for each set of experimental conditions (i.e.,  $100\text{--}500\text{ }\mu\text{N}$  maximum load,  $5\text{--}25\text{ }\mu\text{N/s}$  loading/unloading rate, and  $10\text{--}40\text{ s}$  hold time).

High-load/large-depth indentation tests were performed with a microprobe force apparatus (MFA) described elsewhere (Supporting information). During MFA testing, the sample was kept under mild tension by a steel plate attached to the sample holder by four screws to compensate for sample shrinking by  $10\text{--}20\%$  after cutting. A pre-stress minimizes skin deflection during indentation, reducing the variation in skin property measurement (Butz et al., 2012). All MFA tests were performed with a conospherical diamond-coated tip of  $12.5\text{ }\mu\text{m}$  radius. About 10 samples were used for each set of experimental conditions (i.e.,  $50\text{--}600\text{ mN}$  maximum load,  $5\text{--}90\text{ }\mu\text{m/s}$  depth rate, and  $10\text{--}60\text{ s}$  hold time).

Trapezoidal load profiles were used in all tests. While the specified trapezoidal load profile was observed with relatively shallow indentations (Fig. 2a), in the case of relatively deep indentations, the profile showed nonlinear loading and unloading paths (Fig. 2c), indicating a time-dependent deformation that could not be compensated by the load transducer in a timely fashion. Thus, to maintain a constant loading and unloading rate, depth control was used during the loading and unloading phases of testing, whereas load control was used during the hold time of MFA testing. Since this problem was not encountered with the SFM load transducer, load control was used in all the SFM tests. In some MFA experiments (e.g., Fig. 2a and b), a slight decrease in maximum load was observed during the hold period because the feedback controller could not keep up with the pace of viscoelastic deformation. However, since the load change due to this effect was very small ( $2\text{--}5\%$ ), it may be inferred that a constant-load condition was closely approximated during the hold period.

To obtain insight into time-dependent deformation under constant load (creep tests) for different values of hold time  $t_h$ , loading/unloading rate  $\dot{L} = dL/dt$ , and maximum indentation depth  $h_{max}$  (corresponding to the maximum load  $L_{max}$  applied during the hold time), a creep deformation parameter (creep strain)  $\epsilon_c = (h_f - h_i)/h_i$ , where  $h_i$  and  $h_f$  are the initial and final indentation depths measured at the start and the end of a creep test, respectively, was used to interpret the viscoelastic behavior of skin layers and whole skin. Viscoelastic material constants and elastic contact stiffness of individual skin layers and whole skin were determined by curve fitting the  $\epsilon_c$  data and the contact stiffness,  $S = dL/dh$ , measured at the inception of unloading, respectively, using a best-fit method. However, to accurately measure the elastic contact stiffness, it is necessary to account for viscous effects on the unloading response. Thus, the elastic contact stiffness  $S^e$  was determined from the measured contact stiffness  $S$  at the onset of unloading using the relation (Tang and Ngan, 2003)

$$\frac{1}{S^e} = \frac{1}{S} - \frac{\dot{h}}{\dot{L}_u} \quad (1)$$

where  $\dot{h}$  is the rate of depth change during the hold period (creep test) and  $\dot{L}_u$  is the unloading rate at the inception of unloading.

### 2.4. Statistical analysis

Statistically significant differences between measurements were determined by multiple use of one-way analysis of variance (ANOVA).  $p$ -values were calculated for a significance level  $\alpha = 0.05$ . The null hypothesis (i.e., equal mean at all factor levels) was used to determine if the mean values of different factors (e.g., hold time and loading rate) were statistically different. The null hypothesis was rejected for  $p < 0.05$ .

## 3. Results and discussion

Results presented in this section are for three types of layer/substrate samples: (1) stratum corneum/viable epidermis, (2) dermis/epidermis, and (3) whole skin (with part of the hypodermis as the substrate). Samples were attached to a Petri dish by their substrates. Hereafter, these samples will be referred to as the stratum corneum, dermis, and skin samples, correspondingly. To show general trends, results presented in the form of data points representing mean values and error bars are curve fitted, using the correlation coefficient  $R^2$  to determine the function that best fitted the data.

### 3.1. Time-dependent deformation behavior

SFM testing showed that  $\epsilon_c$  in stratum corneum is not a function of  $t_h$  (Fig. 3a,  $p = 0.870$ ) and tends to marginally increase in the low range of loading rate  $\dot{L}_l$  (Fig. 3b,  $p = 0.055$ ). From the measured  $\epsilon_c$  data, it may be inferred that time-dependent deformation of stratum corneum either did not commence or occurred before the onset of the hold period (i.e., within  $< 10\text{ s}$ ), implying a weak time-dependent deformation of stratum corneum compared to the other skin layers. For  $L_{max} = 350\text{ }\mu\text{N}$ ,  $\epsilon_c$  in stratum corneum is  $\sim 0.20 \pm 0.05$  (Fig. 3a).

MFA testing revealed a time-dependent deformation of dermis and skin. A monotonic increase of  $\epsilon_c$  in dermis from  $\sim 0.08$  to  $\sim 0.25$  was observed with the increase of  $t_h$  in the range  $10\text{--}60\text{ s}$  (Fig. 3c,  $p \approx 0$ ) and increase of  $\dot{h}$  in the  $5\text{--}80\text{ }\mu\text{m/s}$  range (Fig. 3d,  $p \approx 0$ ). The sensitivity of the dermis deformation to the variations of the hold time (Fig. 3c) and the depth rate or indentation speed (Fig. 3d) shows a strong time-dependent deformation behavior.

A similar variation of  $\epsilon_c$  with  $t_h$  was observed with skin (Fig. 3e,  $p \approx 0$ ), i.e.,  $\epsilon_c$  increased from  $\sim 0.12$  to  $\sim 0.32$  with the increase of  $t_h$  by twofold. However, the variation of  $\epsilon_c$  with  $\dot{h}$  significantly differed from that of stratum corneum and dermis, i.e.,  $\epsilon_c$  initially decreased from  $\sim 0.25$  to  $\sim 0.15$  and then increased to  $\sim 0.24$  with  $\dot{h}$  increasing in the range  $5\text{--}30\text{ }\mu\text{m/s}$  (Fig. 3f,  $p \approx 0$ ). For the examined  $\dot{h}$  range, the average  $\epsilon_c$  in the skin is  $\sim 0.216 \pm 0.072$ , which is close to the strain in the stratum corneum (Fig. 3a and b). The initial decrease of  $\epsilon_c$  with the increase of  $\dot{h}$  is attributed to viscoelastic stretching of the skin to accommodate the accumulating deformation, while the increase of  $\epsilon_c$  in the high range of  $\dot{h}$  is associated with gross deformation in the stratum corneum and the upper region of the cellular epidermis, as shown by histology results (Section 3.3). Thus, for the ranges of indentation depth and depth rate investigated, skin deformation is controlled by the stratum corneum, whereas time-dependent deformation of the skin is mainly due to the viscoelastic behavior of the cellular epidermis and the dermis. This is in good agreement with an earlier study (Holt et al., 2008) and in line with attributions of the deformation-rate sensitivity of skin to viscous losses between collagen fibers in the ground substance (Cohen et al., 1976) and within collagen fibrils (Haut, 1983).

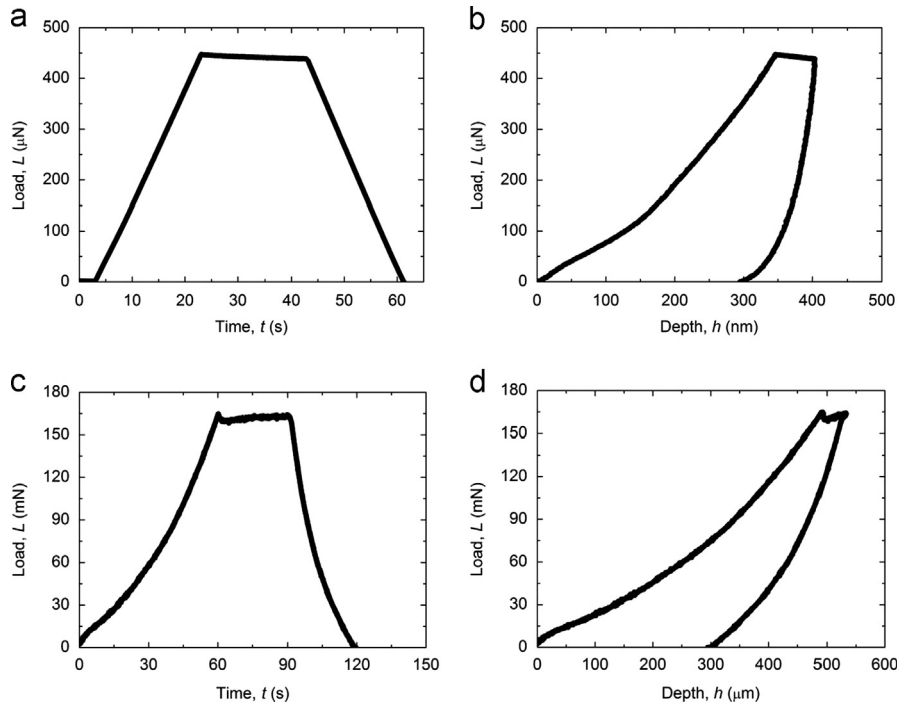


Fig. 2. Indentation load  $L$  versus time  $t$  (left) and depth  $h$  (right) response for loading and unloading rates equal to  $22 \mu\text{N/s}$  and maximum load equal to (a, b)  $450 \mu\text{N}$  and (c, d)  $165 \text{mN}$ .

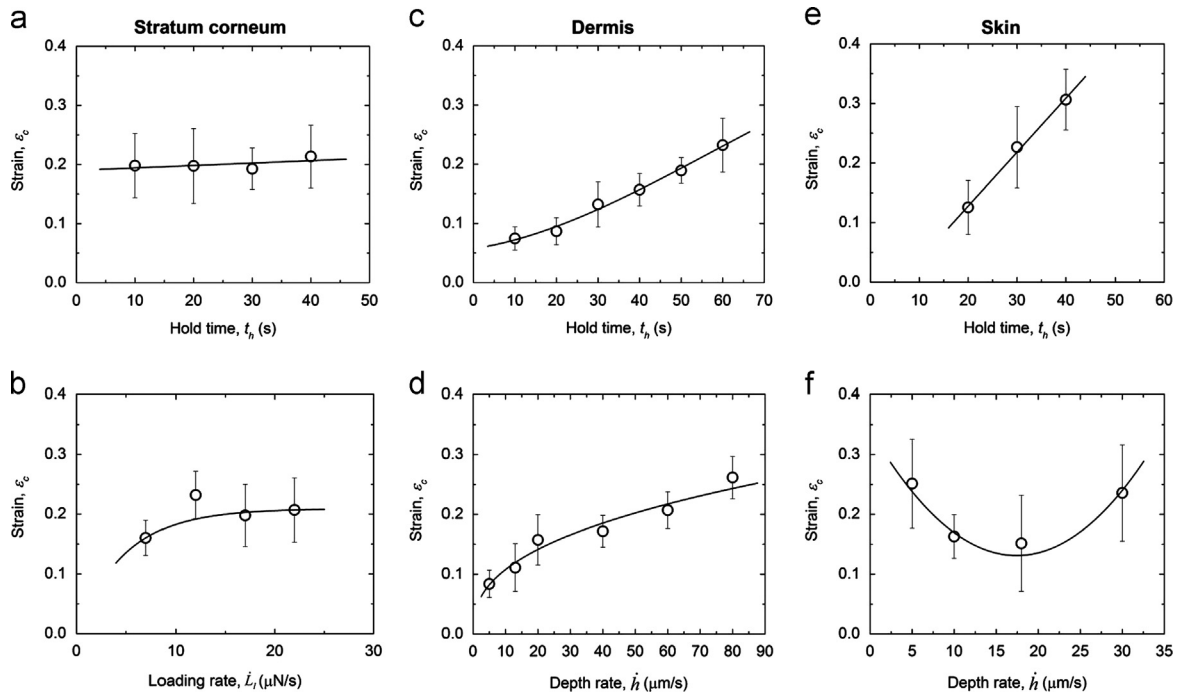


Fig. 3. Strain  $\epsilon_c$  versus (a) hold time  $t_h$  ( $L_{max}=350 \mu\text{N}$ ,  $\dot{L}_l=\dot{L}_u=17 \mu\text{N/s}$ ) and (b) loading rate  $\dot{L}_l$  ( $L_{max}=350 \mu\text{N}$ ,  $t_h=20 \text{s}$ ) for stratum corneum. Strain  $\epsilon_c$  versus (c) hold time  $t_h$  ( $h_0=400 \mu\text{m}$ ,  $\dot{h}=13 \mu\text{m/s}$ ) and (d) depth rate  $\dot{h}$  ( $h_0=400 \mu\text{m}$ ,  $t_h=30 \text{s}$ ) for dermis. Strain  $\epsilon_c$  versus (e) hold time  $t_h$  ( $h_0=150 \mu\text{m}$ ,  $\dot{h}=5 \mu\text{m/s}$ ) and (f) depth rate  $\dot{h}$  ( $h_0=150 \mu\text{m}$ ,  $t_h=30 \text{s}$ ) for skin.

### 3.2. Viscoelastic constants and elastic contact stiffness

A nonlinear variation of the maximum depth  $h_{max}$  with time  $t$  under constant  $L_{max}$  (hold period) was observed with all samples (Fig. 4), with dermis and skin demonstrating similar trends. From a curve-fitting analysis, the function showing the best fit to the  $h_{max}$  data (Fig. 4a, c, and e,  $R^2 \geq 0.99$  for all tests) was found to be of

the following form

$$h_{max} = h_0 + Ct^{1/2} \tag{2}$$

where  $h_0$  is the maximum depth at the start of the hold period ( $t=0$ ) and  $C$  is a viscoelastic material constant determined by curve fitting.

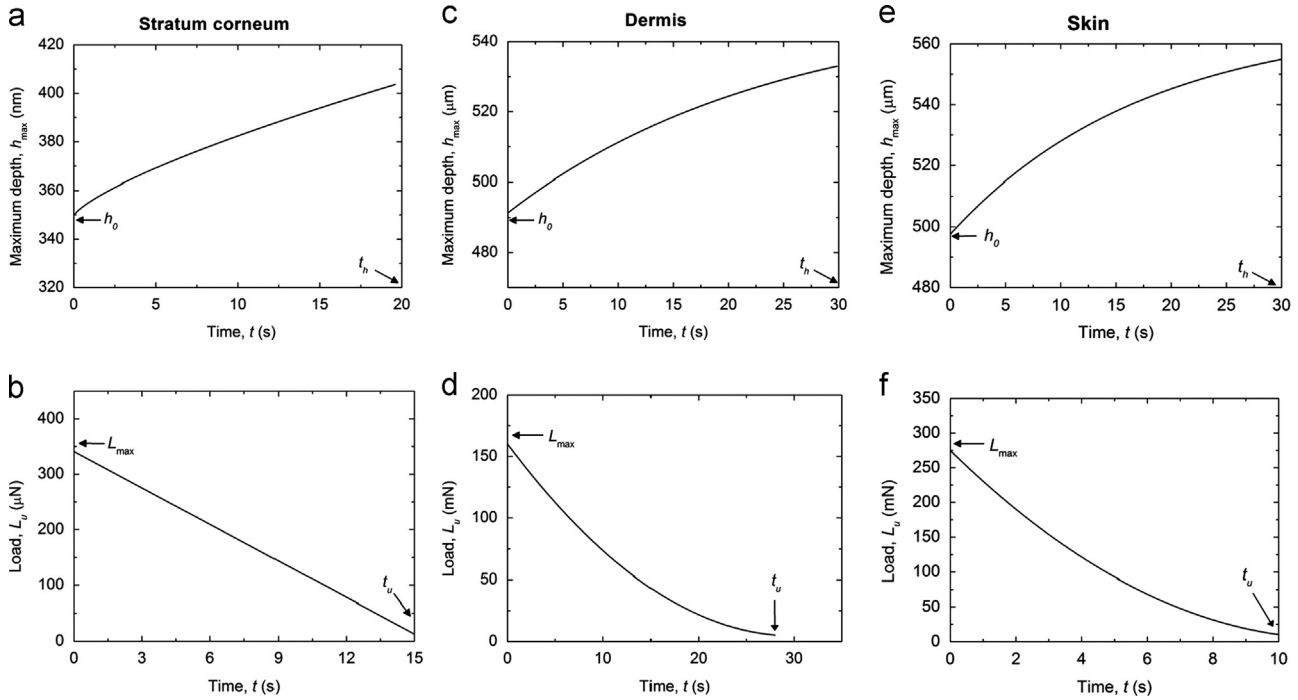


**Fig. 4.** Representative results from single experiments showing the variation of maximum depth  $h_{max}$  with time  $t$  under constant  $L_{max}$  (hold period) for (a) stratum corneum, (c) dermis, and (e) skin, and load  $L$  with time  $t$  during unloading for (b) stratum corneum ( $L_{max}=350 \mu\text{N}$ ), (d) dermis ( $L_{max} \approx 150 \text{ mN}$ ), and (f) skin ( $L_{max} \approx 275 \text{ mN}$ ).

Initial unloading shows a linear load variation with time for stratum corneum (Fig. 4b) and a nonlinear load variation with time for dermis (Fig. 4d) and skin (Fig. 4f). Consequently, for stratum corneum, the initial unloading rate  $\dot{L}_u$  can be obtained as follows:

$$\dot{L}_u = \frac{L_{max} - L}{t} \approx \frac{L_{max}}{t_u} \quad (3)$$

where  $t_u$  is the time for full unloading. Thus, from Eqs. (1)–(3), the elastic contact stiffness of stratum corneum  $S_{sc}^e$  is expressed as follows:

$$S_{sc}^e = \left[ \frac{1}{S} + \frac{C_{sc} t_u}{2 t_h^{1/2} L_{max}} \right]^{-1} \quad (4)$$

where  $C_{sc}$  is the viscoelastic constant of stratum corneum (i.e.,  $C$  in Eq. (2)).

SFM measurements for loading, unloading, and hold times all fixed at 20 s did not show a dependence of  $C_{sc}$  on  $L_{max}$  during the hold period (Fig. 5a,  $p=0.458$ ). From the measured data, the mean value of  $C_{sc}$  is  $20.8 \pm 0.062 \text{ nm/s}^{1/2}$ . These experiments also revealed a nonlinear decrease of  $S_{sc}^e$  (Eq. (4)) with increasing  $h_{max}$  (or  $L_{max}$ ) (Fig. 5b,  $p=0.01$ ). This trend is attributed to the intensifying effect of the soft cellular epidermis with increasing  $h_{max}$ . From measurements obtained in the 400–1200 nm range of  $h_{max}$ , the average  $S_{sc}^e$  is  $\sim 3.47 \pm 0.012 \mu\text{N/nm}$ .

Due to the nonlinear unloading response of dermis (Fig. 5d) and skin (Fig. 5f), the initial unloading rate was obtained as the limit of a second-order polynomial function of time ( $R^2=0.997$ ), i.e.,

$$\dot{L}_u = \lim_{t \rightarrow 0} \left\{ \frac{d}{dt} (L_{max} + D_1 t + D_2 t^2) \right\} \quad (5)$$

where constants  $D_1$  and  $D_2$  can be obtained by curve fitting. Combining Eqs. (1), (2), and (5), the elastic contact stiffness of dermis  $S_{de}^e$  is expressed as follows:

$$S_{de}^e = \left[ \frac{1}{S} + \frac{C_{de}}{2 D_{de} t_h^{1/2}} \right]^{-1} \quad (6)$$

where  $C_{de}$  and  $D_{de}$  are the dermis viscoelastic constants  $C$  and  $D_1$  in Eqs. (2) and (5), respectively.

MFA tests performed with dermis samples for  $\dot{h}=10 \mu\text{m/s}$  and  $t_h=40 \text{ s}$  showed a strong dependence of the dermis viscoelastic behavior and elastic contact stiffness on  $L_{max}$  and  $h_{max}$ , respectively. In particular,  $C_{de}$  initially increased from 6 to  $16 \mu\text{m/s}^{1/2}$  in the range  $\sim 25 \leq L_{max} \leq 230 \text{ mN}$  and then decreased to a plateau of  $\sim 9 \mu\text{m/s}^{1/2}$  for  $L_{max} \geq 400 \text{ mN}$  (Fig. 5c,  $p \approx 0$ ), while  $S_{de}^e$  increased monotonically in the range  $150 \leq h_{max} \leq 550 \mu\text{m}$  (Fig. 5d,  $p \approx 0$ ). It is noted that the critical depth ( $h_{max}=400 \mu\text{m}$ ) beyond which  $S_{de}^e$  sharply increases correlates with  $L_{max}=230 \text{ mN}$ , which corresponds to the peak value of  $C_{de}$ . The increase of  $C_{de}$  in the range  $0 \leq L_{max} \leq 230 \text{ mN}$  is attributed to the intensifying viscoelastic behavior of dermis with increasing load, while the gradual decrease of  $C_{de}$  for  $L_{max} \geq 230 \text{ mN}$  is due to the squeeze-out of fluid from the compressed dermis, which becomes significant above a critical load (pressure). This explanation is in agreement with the trend of  $S_{de}^e$  to sharply increase for  $h_{max} \geq 400 \mu\text{m}$  (i.e.,  $L_{max} \geq 230 \text{ mN}$ ) due to the significant loss of fluid from the dermis. The fact that  $C_{de}$  (Fig. 5c) is about three orders of magnitude higher than  $C_{sc}$  (Fig. 5a) implies a dominant dermis effect on skin viscoelasticity, whereas the asymptotic increase of  $S_{de}^e$  (Fig. 5d) toward values approaching those of  $S_{sc}^e$  (Fig. 5b) indicates a dominant effect of stratum corneum on the elastic contact stiffness of skin. Thus, time-dependent deformation is mostly due to the dermis, while elastic contact stiffness is mainly provided by the stratum corneum.

Considering the similar elastic contact behavior of dermis and skin, the elastic contact stiffness of skin  $S_{sk}^e$  can be expressed by a relation similar to that given by Eq. (6), i.e.,

$$S_{sk}^e = \left[ \frac{1}{S} + \frac{C_{sk}}{2 D_{sk} t_h^{1/2}} \right]^{-1} \quad (7)$$

where  $C_{sk}$  and  $D_{sk}$  are the skin viscoelastic constants  $C$  and  $D_1$  in Eqs. (2) and (5), respectively.  $C_{sk}$  shows an increasing trend similar to that of dermis up to  $L_{max} \approx 130 \text{ mN}$ , a plateau of  $\sim 11.5 \mu\text{m/s}^{1/2}$  in the intermediate range  $130 \leq L_{max} \leq 350 \text{ mN}$ , and a tendency to increase for  $L_{max} > 350 \text{ mN}$  (Fig. 5e,  $p \approx 0$ ).  $S_{sk}^e$  demonstrates a

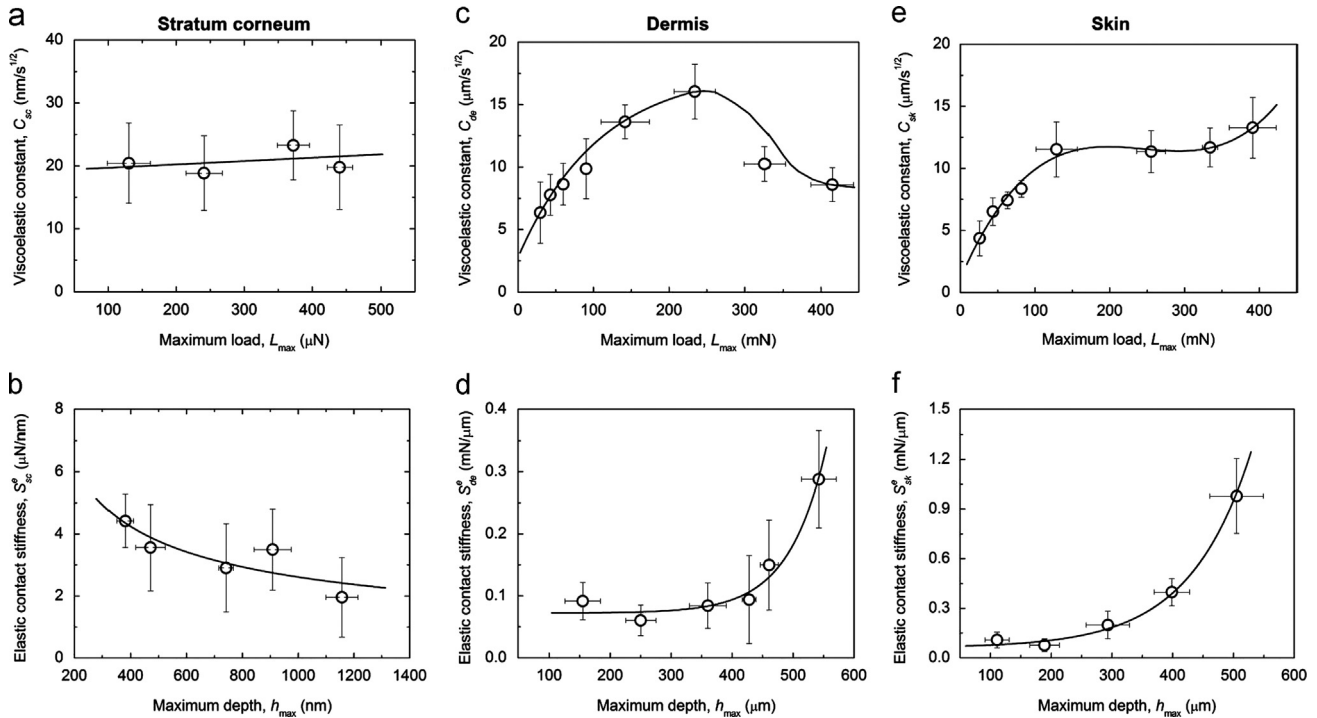


**Fig. 5.** (a) Viscoelastic constant of stratum corneum  $C_{sc}$  versus maximum load  $L_{max}$  and (b) elastic contact stiffness of stratum corneum  $S_{sc}^e$  versus maximum depth  $h_{max}$  ( $t_l = t_u = t_h = 20$  s). (c) Viscoelastic constant of dermis  $C_{de}$  versus maximum load  $L_{max}$  and (d) elastic contact stiffness of dermis  $S_{de}^e$  versus maximum depth  $h_{max}$  ( $t_l = 40$  s,  $\dot{h} = 10$  μm/s). (e) Viscoelastic constant of skin  $C_{sk}$  versus maximum load  $L_{max}$  and (f) elastic contact stiffness of skin  $S_{sk}^e$  versus maximum depth  $h_{max}$  ( $t_l = 40$  s,  $\dot{h} = 10$  μm/s).

trend very similar to that of dermis, assuming values between those of the dermis and stratum corneum (Fig. 5f,  $p \approx 0$ ). For  $h_{max} \leq 190$  μm,  $S_{sk}^e \approx 0.09$  mN/μm, which is close to  $S_{de}^e$  in the same range (Fig. 5d), whereas for  $h_{max} > 190$  μm,  $S_{sk}^e$  assumes much higher values, which are close to those asymptotically approached by  $S_{sc}^e$  in the same range (i.e., on the order of  $\sim 1$  mN/μm or  $\sim 1$  μN/nm). Thus,  $S_{sk}^e$  demonstrates a dramatic increase with  $h_{max}$  (by about an order of magnitude), with  $S_{de}^e$  and  $S_{sc}^e$  representing lower and upper bounds, respectively. For  $h_{max} \leq 190$  μm (Fig. 5f),  $S_{sk}^e$  is in fair agreement with reported skin stiffness data (Frick et al., 2001), while the significantly higher  $S_{sc}^e$  than  $S_{de}^e$  (and  $S_{sk}^e$ ) is consistent with the three times higher epidermis stiffness than that of the dermis (Lamers et al., 2013).

### 3.3. Cross-sectional histology

Cross-sectional histology of whole skin provided additional insight into the deformation behavior of different skin layers. Because obtaining cross-sectional samples from the indented skin specimens is extremely cumbersome, slow speed (5 μm/s) scratch tests were performed with the MFA in the 50–400 mN load range, and cross-sectional samples were obtained perpendicular to the residual scratch produced on skin samples. Although the loads applied in these tests do not exactly match  $L_{max}$  applied during the hold period, the histology results provide a useful qualitative means of evaluating the role of stratum corneum, cellular epidermis, and dermis in skin deformation and shear-induced damage. For relatively low loads (i.e., 50 mN), deformation leads to shallow sinking of the skin tissue without excessive damage in the epidermis and/or delamination at the stratum corneum/cellular epidermis interface (Fig. 6a). Dark-red spots in the dermis represent hard fibrils and nuclei. The absence of notable changes in the epidermis suggests that skin deformation due to low-load scratching is mainly controlled by the dermis.

Significant skin damage was observed with intermediate loads (e.g., 200 mN). In addition to more pronounced sinking of the skin, excessive cohesive failure and delamination of the hard stratum corneum from the soft cellular epidermis occurred (Fig. 6b), apparently due to the development of high tensile stresses in the downward bending stratum corneum and the significant mismatch of the viscoelastic–plastic properties of stratum corneum and cellular epidermis. Skin scratching under high loads (e.g., 400 mN) resulted in severe scarring of the skin, characterized by the complete removal of the stratum corneum and cellular epidermis (Fig. 6c).

The deformation behavior revealed by the histology results provides an explanation for the viscoelastic response and elastic contact stiffness of skin (Fig. 5e and f, respectively). Because low-load skin deformation is mainly controlled by dermis deformation (Fig. 6a), in the low range of  $L_{max}$  and  $h_{max}$ ,  $C_{sk}$  and  $S_{sk}^e$  are mainly affected by  $C_{de}$  (Fig. 5c) and  $S_{de}^e$  (Fig. 5d), respectively. In the intermediate range of  $L_{max}$ ,  $C_{sk}$  remains almost constant because skin deformation is controlled by the deformation in the stratum corneum, which exhibits relatively insignificant viscoelastic behavior (Figs. 3a and 5a). Both  $C_{sk}$  and  $S_{sk}^e$  increase in the high range of  $L_{max}$  and  $h_{max}$ , respectively, due to the enhanced viscous behavior of dermis at high contact pressures.

### 3.4. Creep and stress relaxation

Creep tests (five samples,  $L = 90$  mN) revealed a viscoelastic–plastic response, represented by a rheological model comprising elastic, steady-state creep, and transient creep elements (Fig. 7a). The sharp depth decrease upon full unloading ( $t = 300$  s) is mostly attributed to the stratum corneum, whereas the subsequent transient creep (recovery) is mainly due to the viscoelastic behavior of the cellular epidermis and the dermis. From 25 creep tests, it was found that  $C_{de} = 10.42 \pm 0.844$  μm/s<sup>1/2</sup>, which is in good agreement with the value determined from short-term tests



## References

- Archer, C.B., 2010. Functions of the skin. In: Burns, T., Breathnach, S., Cox, N., Griffiths, C. (Eds.), *Rook's Textbook of Dermatology*, eighth edition, Wiley-Blackwell, Oxford, UK, pp. 4.1–4.11.
- Avon, S.L., Wood, R.E., 2005. Porcine skin as an *in-vivo* model for ageing of human bite marks. *J. Forensic Odonto-Stomatology* 23, 30–39.
- Butz, K.D., Griebel, A.J., Novak, T., Harris, K., Kornokovich, A., Chiappetta, M.F., Neu, C.P., 2012. Prestress as an optimal biomechanical parameter for needle penetration. *J. Biomech.* 45, 1176–1179.
- Cohen, R.E., Hooley, C.J., McCrum, N.G., 1976. Viscoelastic creep of collagenous tissue. *J. Biomech.* 9, 175–184.
- Crichton, M.L., Donose, B.C., Chen, X., Raphael, A.P., Huang, H., Kendall, M.A.F., 2011. The viscoelastic, hyperelastic and scale dependent behavior of freshly excised individual skin layers. *Biomaterials* 32, 4670–4781.
- Crichton, M.L., Chen, X., Huang, H., Kendall, M.A.F., 2013. Elastic modulus and viscoelastic properties of full thickness skin characterized at micro scales. *Biomaterials* 34, 2087–2097.
- Frick, T.B., Marucci, D.D., Cartmill, J.A., Martin, C.J., Walsh, W.R., 2001. Resistance forces acting on suture needles. *J. Biomech.* 34, 1335–1340.
- Fry, P., Harkness, M.L.R., Harkness, R.D., 1964. Mechanical properties of the collagenous framework of skin in rats of different ages. *Am. J. Physiol.* 206, 1425–1429.
- Geerligs, M., van Breemen, L., Peters, G., Ackermans, P., Baaijens, F., Oomens, C., 2011. *In vitro* indentation to determine the mechanical properties of epidermis. *J. Biomech.* 44, 1176–1181.
- Gibson, T., Stark, H., Evans, J.H., 1969. Directional variation in extensibility of human skin *in vivo*. *J. Biomech.* 2, 201–204.
- Glaser, A.A., Marangoni, R.D., Must, J.S., Beckwith, T.G., Brody, G.S., Walker, G.R., White, W.L., 1965. Refinements in the methods for the measurement of the mechanical properties of unwounded and wounded skin. *Med. Electron. Biol. Eng.* 3, 411–419.
- Groves, R.B., Coulman, S.A., Birchall, J.C., Evans, S.L., 2012. Quantifying the mechanical properties of human skin to optimize future microneedle device design. *Comput. Methods Biomech. Biomed. Eng.* 15, 73–82.
- Haut, R.C., 1983. Age-dependent influence of strain rate on the tensile failure of rat-tail tendon. *ASME J. Biomech. Eng.* 105, 296–299.
- Holt, B., Tripathi, A., Morgan, J., 2008. Viscoelastic response of human skin to low magnitude physiologically relevant shear. *J. Biomech.* 41, 2689–2695.
- Lamers, E., van Kempen, T.H.S., Baaijens, F.P.T., Peters, G.W.M., Oomens, C.W.J., 2013. Large amplitude oscillatory shear properties of human skin. *J. Mech. Behav. Biomed. Mater.* 28, 462–470.
- McGrath, J.A., Uitto, J., 2010. Anatomy and organization of human skin. In: Burns, T., Breathnach, S., Cox, N., Griffiths, C. (Eds.), *Rook's Textbook of Dermatology*, eighth edition, Wiley-Blackwell, Oxford, UK, pp. 3.1–3.53.
- Schmook, F.P., Meingassner, J.G., Billich, A., 2001. Comparison of human skin or epidermis models with human and animal skin in *in-vitro* percutaneous absorption. *Int. J. Pharm.* 215, 51–56.
- Shergold, O.A., Fleck, N.A., Radford, D., 2006. The uniaxial stress versus strain response of pig skin and silicone rubber at low and high strain rates. *Int. J. Impact Eng.* 32, 1384–1402.
- Tang, B., Ngan, A.H.W., 2003. Accurate measurement of tip-sample contact size during nanoindentation of viscoelastic materials. *J. Mater. Res.* 18, 1141–1148.
- Yuan, Y., Verma, R., 2006. Measuring microelastic properties of stratum corneum. *Colloids Surf. B: Biointerfaces* 48, 6–12.
- Zak, M., Kuroopka, P., Kobielarz, M., Dudek, A., Kaleta-Kuratewicz, K., Szotek, S., 2011. Determination of the mechanical properties of the skin of pig fetuses with respect to its structure. *Acta Bioeng. Biomech.* 13, 37–43.